AIAA'86

AIAA-86-1054

Computational Study of the Effect of Base Slant

K. Tsuboi, Japan Information Service, Ltd., Tokyo, Japan;
R. Himeno, Nissan Motor Co., Ltd., Yokosuka, Japan;
S. Shirayama, The University of Tokyo, Japan;
K. Kuwahara, The Institute of Space and Astronautical Science, Tokyo, Japan

AIAA/ASME 4th Fluid Mechanics, Plasma Dynamics and Lasers Conference
May 12-14, 1986/Atlanta, GA

COMPUTATIONAL STUDY OF THE EFFECT OF BASE SLANT

Kazuhiro Tsuboi
Japan Information Service, Ltd.
Kita-Aoyama, Minato-ku, Tokyo, Japan

Ryutaro Himeno
Central Engineering Laboratories, Nissan Motor Co., Ltd.
Yokosuka, Kanagawa, Japan

Susumu Shirayama
Department of Aeronautics, The University of Tokyo
Hongo, Bunkyo-ku, Tokyo, Japan

Kunio Kuwahara
The Institute of Space and Astronautical Science
Komaba, Meguro-ku, Tokyo, Japan

Abstract

Flow fields around a circular cylinder with a slanted base placed its axis parallel to the uniform flow are investigated numerically by solving the three-dimensional incompressible Navier-Stokes equations. Two typical separation patterns are simulated successfully. The dependence of the drag coefficient on the base slant angle was found to agree qualitatively with experiments; especially drastical change of the drag coefficient at the critical angle of slant base is captured.

Introduction

Flow around a circular cylinder with a slanted base is complicated and depends on the geometric parameters strongly[1]. Among them, the slant base angle as shown in Fig.1 is the most important. This parameter has a critical value, at which the flow pattern in the wake changes completely. When the slant base angle is smaller than the critical value, the flow pattern is quasi-axisymmetric and is characterized by a closed separation region. On the other hand, the wake structure for a larger value is fully three dimensional and is characterized by a pair of streamwise vortex tubes originated from the base surface. It is observed by experiments that the drag coefficient changes drastically at a certain base angle; this change is supposed to be due to the difference of the above flow patterns.

In the present paper, three-dimensional flow after a circular cylinder with a slanted base is investigated by solving the incompressible Navier-Stokes equations using finite-difference method. The computational method is based on the Helmholtz decomposition. The third-order upwind scheme is used for the differentiation of the nonlinear terms, which was successfully applied to the flow around a circular cylinder at critical Reynolds number[2], to a turbulent channel flow[3] and to flows around a bluff body[4].

Computational scheme

The three-dimensional incompressible Navier-Stokes equations written in a generalized coordinate system are solved by finite-difference method.

Poisson equation for pressure is derived from the basic equations based on the Helmholtz decomposition[5)-6)] and is solved at every time step.

The Euler implicit scheme is used for the time integration of Navier-Stokes equations. All spatial derivatives except those of the nonlinear terms are approximated by central differences. The nonlinear terms are approximated by the follwing third-order upwind scheme:

$$\left(u\frac{\partial u}{\partial x}\right)_i =$$

$$u_i(-u_{i+2} + 8(u_{i+1} - u_{i-2}) + u_{i-2})/12h$$

$$+|u_i|(u_{i+2}-4u_{i+1}+6u_i-4u_{i-1}+u_{i-2})/4h \quad (1)$$

The finite-difference equations are obtained by discretizing the above equations. The resulting equations are solved by successive over relaxation method. The computations were done on a supercomputer Fujitsu VP-200, the maximum speed of which is 570 M FLOPS. The computation time is about three hours per case.

Grid system

The grid was generated as follows: at first, outer and inner boundaries were specified and the initial grid was generalized by interpolating linearly. Next, the grid was concentrated depending on the Reynolds number[7] so that sufficient grid points are situated in the boundary layer. Finally, orthogonalization of the grid near body was performed by the algebraic method[8].

Fig.2(a) shows the global view of the grid system for the base slant angle of 50 degrees. Fig.2(b)(c) show the grid near the nose and the base, respectively.

Results

In all calculations, Reynolds number based on a diameter of a circular cylinder is equal to 10,000 and impulsive start was used.

(1) Base slant angle 40 degrees.

Figures 3 and 4 show a flow field at t=20.0 and t=50.0, respectively. In Fig.3 a pair of vortex tubes are observed, which is not symmetric yet. A pair of vortex tubes appears initially and grows for a while; but they gradually become weaker. Instead, a dead water region emerges and develops downstream, which is characterized by a quasi-axisymmetric separation pattern as shown in Fig.4.

(2) Base slant angle 50 degrees

Figure 5 shows flow field at t=20.0. A pair of vortex tubes is formed. As the flow field develops, the basic structure does not change much and a pair of vortex tubes remains as shown in Fig.6. This flow field gives the spiral trajectory of particles which is similar to the photographs taken by Chometon[9]. Figure 7 shows the particle paths and pressure distribution on the base surface in the case of $\alpha = 40^{\circ}$ and $\alpha = 50^{\circ}$, where for ease of understanding, particles originated on right half surface of the base are cut out by the way. This makes the difference of the two flow fields clear.

(3) Base slant angle 0 degree

In this case, the body geometry is axisymmetric. Figure.8 and 9 show an equi-pressure surface at t=4.0 and t=55.0, respectively. At initial stage, vortex ring is formed, the structure of which is symmetric completely as shown in Fig.8. As time goes on, however, the wake develops to asymmetric as shown in Fig.9.

(4) Drag coefficient

Figure 10 shows the variation of the drag coefficient with the slant base angle. The critical change takes place at about 48 degrees. The coefficient is near flat at 0.08 for the smaller value of base angle and reduces from 0.12 as increasing the base angle for the larger.

Conclusion

Flows parallel to a circular cylinder with a slanted base were investigated numerically and they were visulalized extensively to see the flow structure. Initially, flow field is characterized by a pair of vortex tubes. It is found that this structure is not stable and that flow field behind the base develops to quasi-axisymmetric structure when the base angle is smaller than the critical one. Especially, when the body geometry is axisymmetric, vortex ring is formed, which is broken finally. On the other hand, at a larger base angle a pair of streamwise vortex tubes sticks on the slanted base and this flow structure is rather stable.

The variation of drag coefficient was calculated as a function of the slant base angle, which suggests the critical angle. The local maximum value takes between the slant base angle 45 and 55 degrees, where the drag coefficient changes strongly.

References

1) T. Morel: "The Effect of Base Slant on the Flow Pattern and Drag of Three-Dimensional Bodies with Blunt Ends", Aerodynamic Drag Mechanisms of Bluff Bodies and Road Vehicles, 1978.

2) T. Kawamura and K. Kuwahara: "Computation of High Reynolds Number Flow around a Circular Cylinder with Surface Roughness", AIAA-84-0340.

3) T. Kawamura and K. Kuwahara: "Direct Simulation of a Turbulent Inner Flow by Finite Difference Method", AIAA-85-0376.

4) R. Himeno, S. Shirayama, K. Kamo and K. Kuwahara: "Computational Study of Three-Dimensional Wake Structure", AIAA-85-1617.

5) A. J. Chorin: "Numerical Solution of the Navier-Stokes Equations", Math. Comp. 22, 1968.

6) H. Takami and K. Kuwahara: "Numerical study of three-dimensional flow within a cubic cavity", J. Phys. Soc. Japan 37, 1974.

7) D. A. Anderson, J. C. Tannehill and R. H. Pletcher: "Computational Fluid Mechanics and Heat Transfer", McGRAW-HILL, 1984.

8) S. Obayashi, K. Matsushima, K. Fujii and K. Kuwahara: "Improvement in Efficiency and Reliability for Navier-Stokes Computations Using the LU-ADI Factorization Algorithm", AIAA-86-0338.

9) F. Chometon: "Calculating Three-Dimensional Separated Flow around Road Vehicles", International Journal of Vehicle Design, Technological Advances in Vehicle Design Series, SP3, Impact of Aerodynamics on Vehicle Design, 1983.

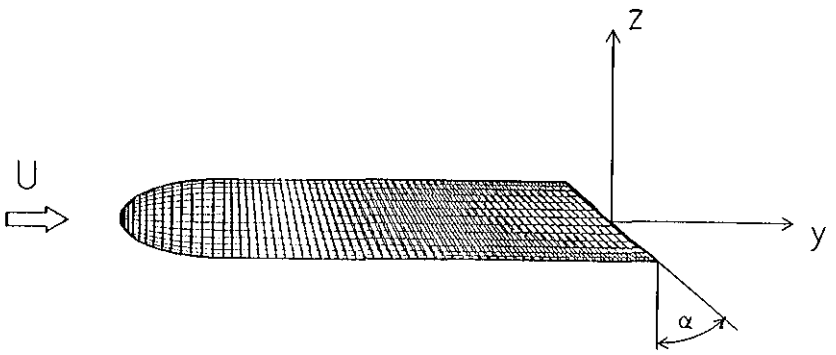

Fig.1 Configuration of the slanted base

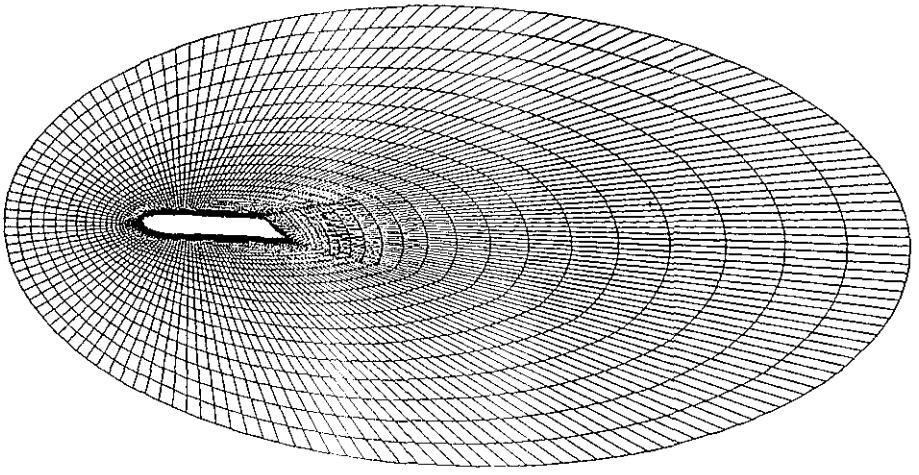

(a) Global view

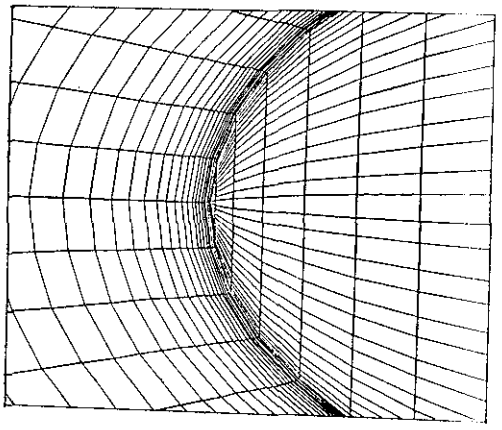

(b) Grid near the nose

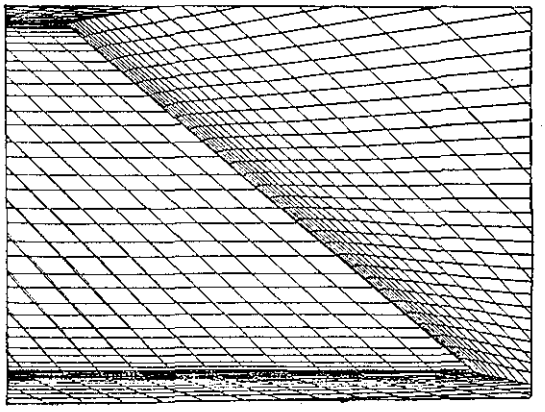

(c) Grid near the base

Fig.2 Grid system (80x33x40)

(a) Top view of equi-pressure surface

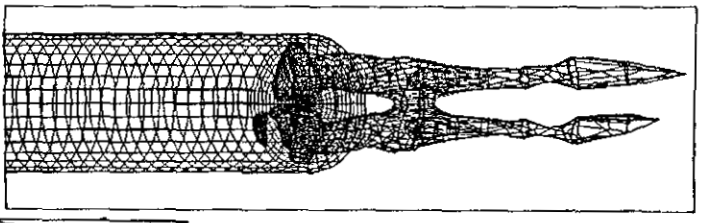

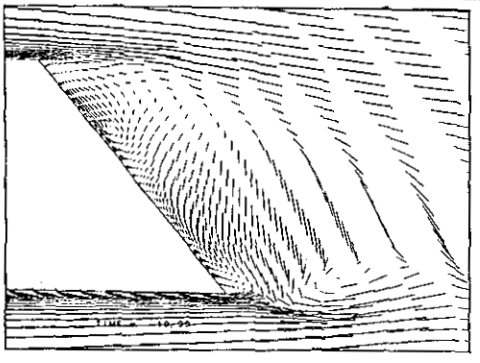

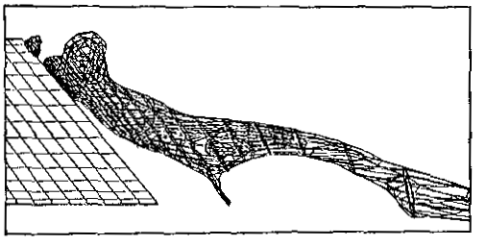

(c) Side view of equi-pressure surface

(b) Velocity distribution on y-z plane

Fig.3 Flow field in the case of base angle 40° (t=20.0)

(a) Top view of equi-pressure surface

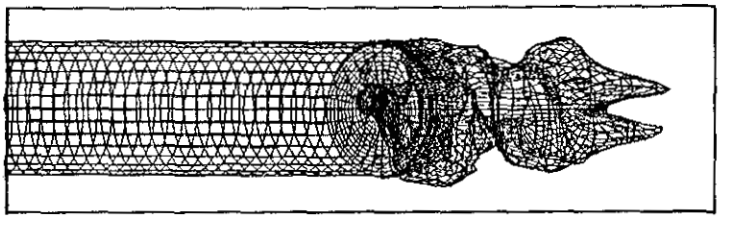

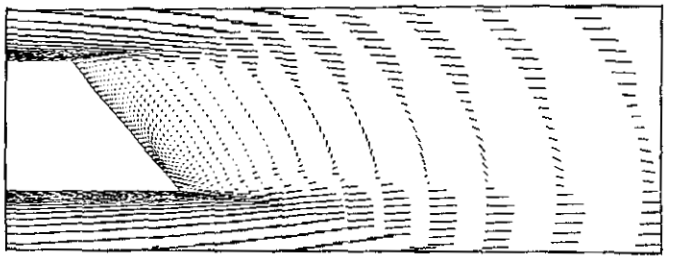

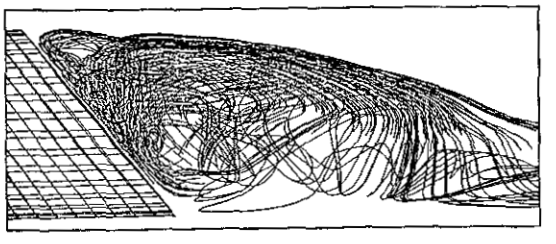

(b) Velocity distribution on y-z plane

(d) Side view of particle paths

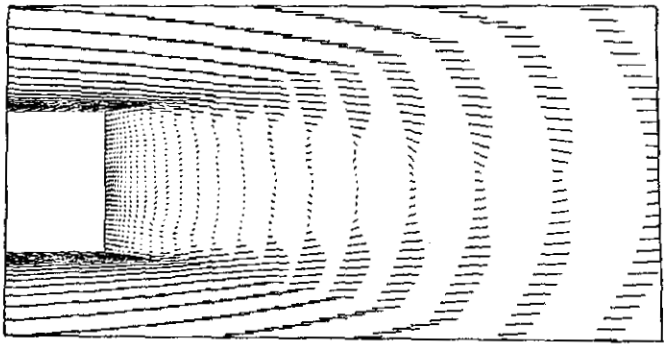

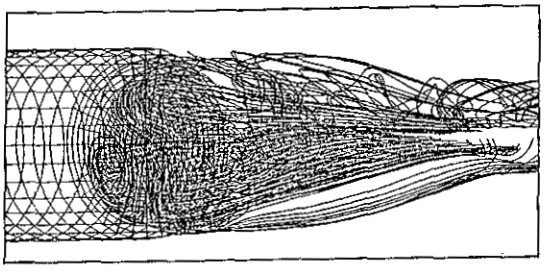

(e) Top view of particle paths

(c) Velocity distribution on x-y plane

Fig.4 Flow field in the case of base angle 40° (t=50.0)

(a) Top view of equi-pressure surface

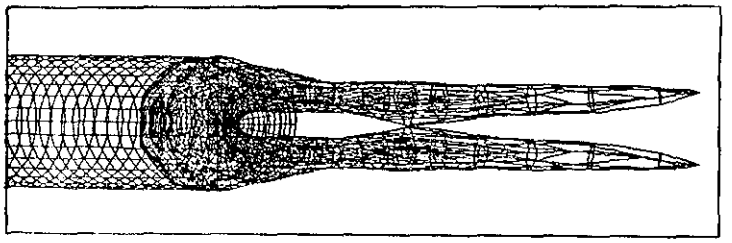

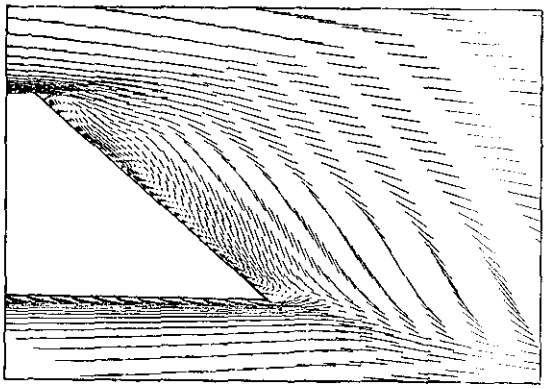

(b) Velocity distribution on y-z plane

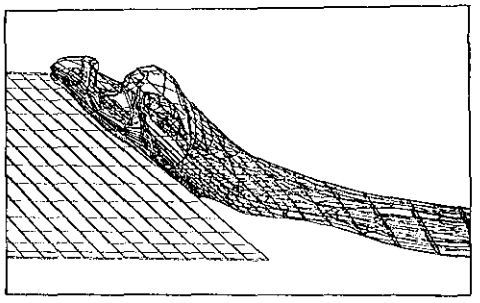

(c) Side view of equi-pressure surface

Fig.5 Flow field in the case of base angle 50° (t=20.0)

(a) Top view of equi-pressure surface

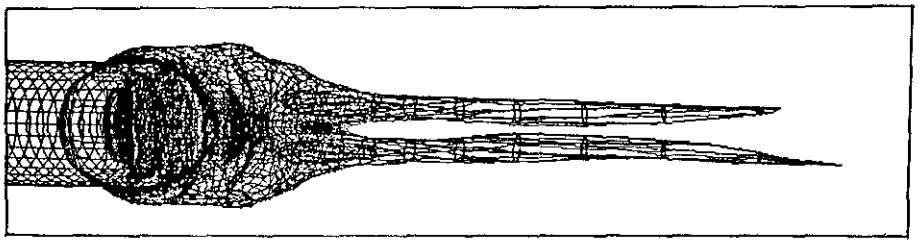

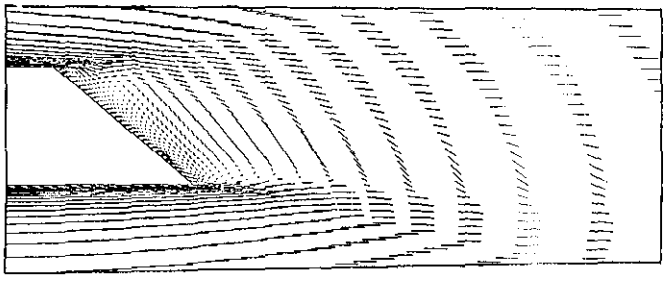

(b) Velocity distribution on y-z plane

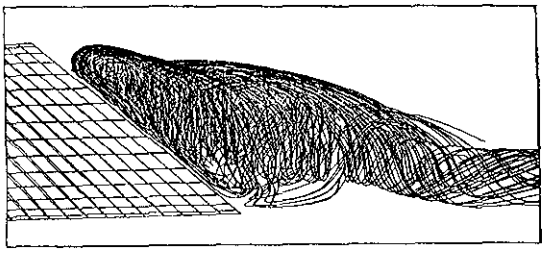

(d) Side view of particle paths

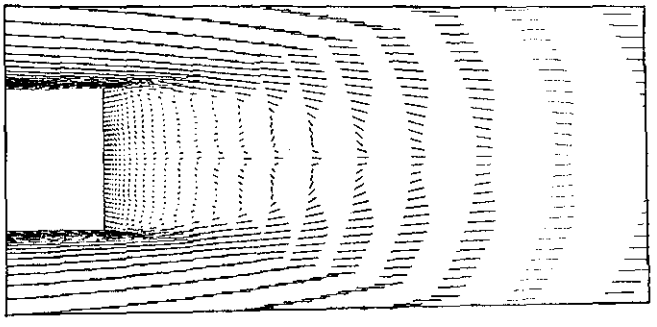

(c) Velocity distribution on x-y plane

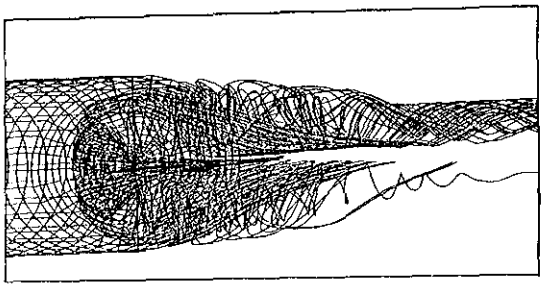

(e) Top view of particle paths

Fig.6 Flow field in the case of base angle 50° (t=50.0)

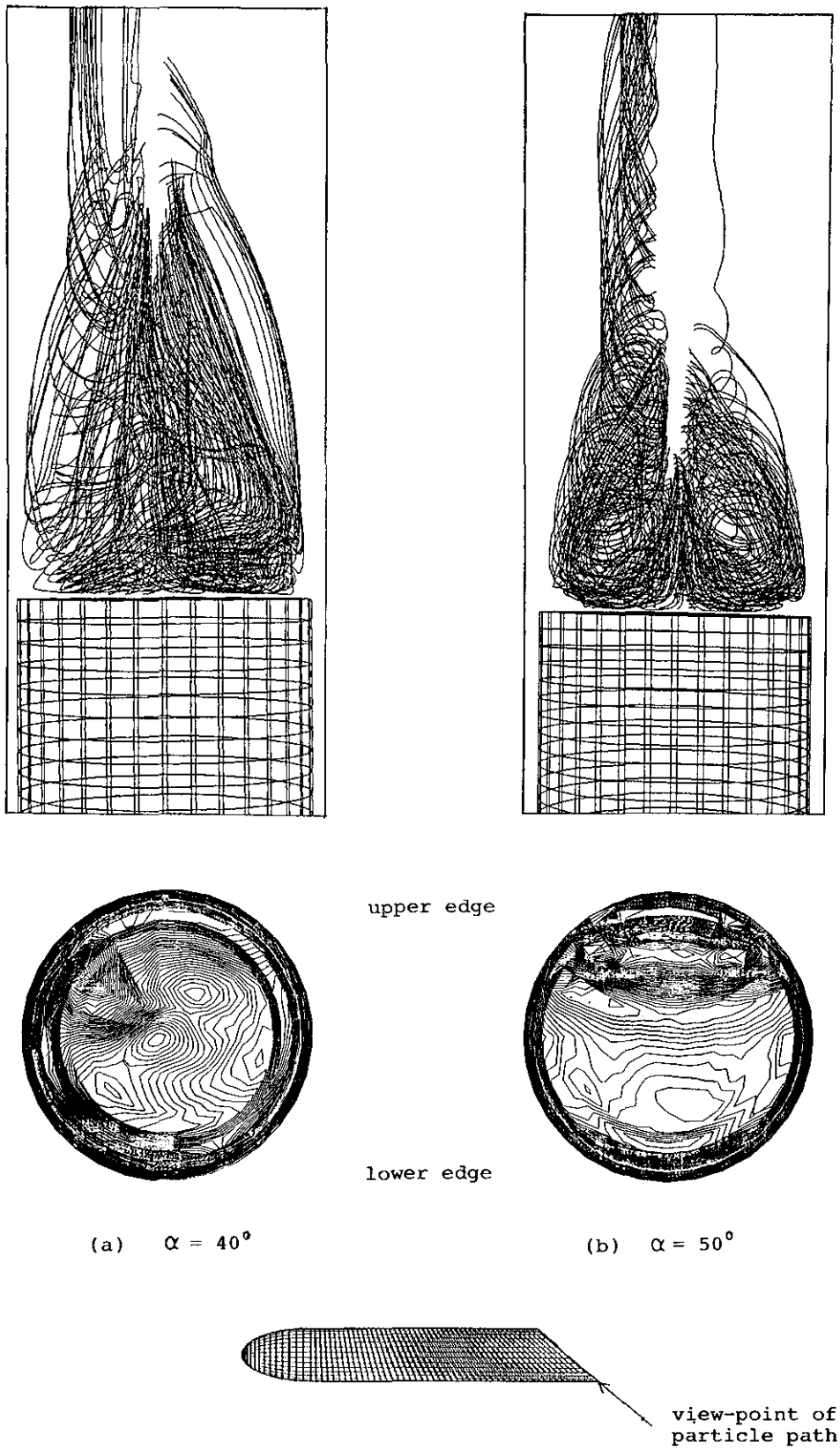

Fig.7 Particle paths and pressure distribution on the base

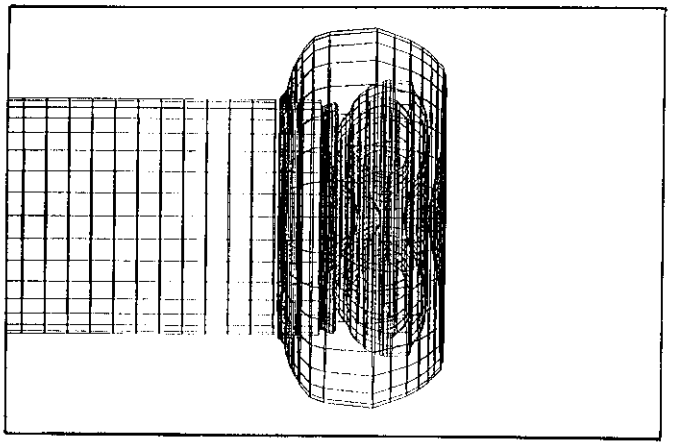

Fig.8 Equi-pressure surface of 0^0 base angle (t=4.0)

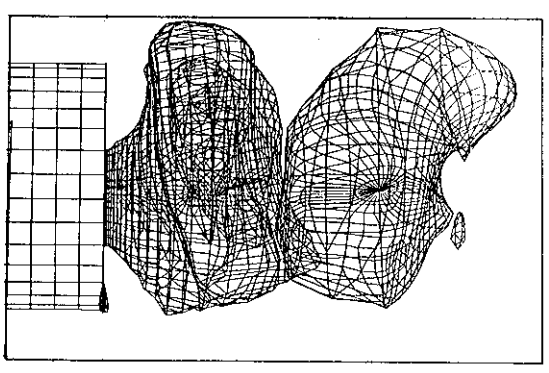

(a) Top view

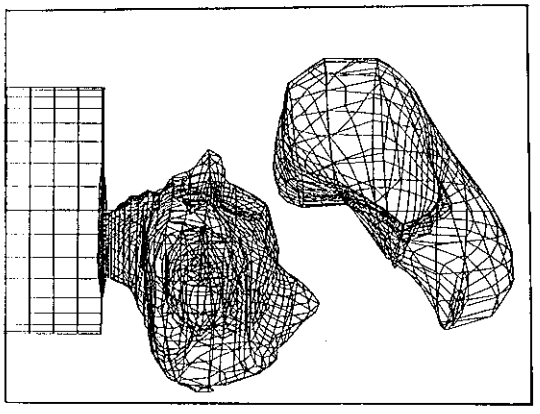

(b) Side view

Fig.9 Equi-pressure surface of 0^0 base angle (t=55.0)

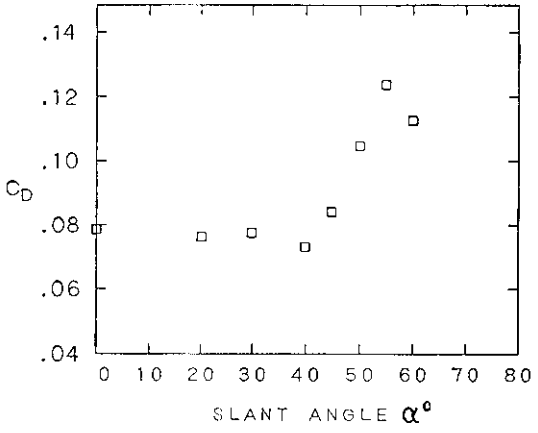

Fig.10 Drag-coefficient variation with slant angle